Spin-Freezing Temperature of Some Oxide and Fluoride Glasses Containing Iron (III)

By

Katsuhisa TANAKA*, Kazuyuki HIRAO* and Naohiro SOGA*

(Received June 27, 1990)

Abstract

The magnetic transition observed in iron-containing oxide and fluoride glasses where antiferromagnetic interactions are dominant among the iron ions has been discussed on the basis of the superparamagnetic model. The theoretical approach based on the model proposed by Shtrikman and Wohlfarth has revealed that the spin-freezing temperature of the oxide and fluoride glasses increases with the increase of the average value of the superexchange interaction . This suggests that the spin-freezing temperature increases with the increase of the covalency of Fe-O or Fe-F bond when the content of the iron ions is identical. The relation between the spin-freezing temperature and the isomer shift value obtained experimentally for some oxide and fluoride glasses seems to support this expectation.

1. Introduction

It has been known that most of the oxide and fluoride glasses containing a relatively large amount of magnetic ions show a magnetic transition like that of cluster spin glasses or mictomagnets. Verhelst et al.[1] first explained the cluster spin glass behavior of cobalt and manganese aluminosilicate glasses in terms of the superparamagnetic model. They assumed that there exist monodomains where cobalt or manganese ions are concentrated in the glass, and connected the phenomenon that a maximum appeared in the susceptibility vs. temperature curve when the zero field cooling was applied with a progressive freezing of the monodomains in a superparamagnetic fashion. The susceptibility vs. temperature curve they reproduced theoretically was in a qualitative agreement with that obtained experimentally. Since then, this model has been often applied to explain several magnetic properties of oxide glasses. For instance, Rechenberg et al.[2] explicated the experimental fact that the remnant magnetization varies with logarithm of the time for $83.1CoO \cdot 15.5Al_2O_3 \cdot 1.4\,SiO_2$ glasses by using the superparamagnetic

* Department of Industrial Chemistry, Faculty of Engineering, Kyoto University, Sakyo-ku, Kyoto 606, Japan

domain model. Jamet et al.[3] examined the temperature dependence of the ESR line shift and the linewidth for $Mn_3Al_2Si_3O_{12}$ glasses, and concluded that the freezing of each spin takes place progressively in the temperature range of 10 to 3.6 K. This model was also utilized to interpret the magnetic transition of some metallic spin glasses. Wohlfarth[4] attempted to clarify the spin-freezing temperature of some spin glasses including metallic ones in terms of the anisotropy field which determines the direction of the magnetization in a cluster. Burke et al.[5] described the magnetic structure of CrFe alloys containing 16.7 to 25 at % Fe on the basis of the simple superparamagnetism. However, as Burke et al.[5] pointed out, the simple superparamagnetic model is insufficient for understanding the magnetic behavior of those cluster spin glasses fully, because the cluster existing in those spin glasses is the percolation cluster, whose volume varies with temperature rather than the single-domain fine particle treated in the superparamagnetism by Néel[6], and the intercluster interaction exists. The importance of considering the variation of the cluster size with temperature and the interaction between clusters has also been pointed out for some cluster spin glasses such as Fe_xNiGe[7] and amorphous FeO-Al_2O_3-SiO_2[8]. Theoretical treatment of these problems was firstly carried out by Shtrikman and Wohlfarth[9,10]. They introduced a parameter T_0, temperature corresponding to the intercluster interaction, and gave a physical meaning to the Vogel-Fulcher empirical relation which holds in the measuring frequency dependence of the spin-freezing temperature, The Shtrikman-Wohlfarth model, however, has not been applied yet to oxide and fluoride glasses where a distribution of superexchange interaction is expected to exist.

In the present study, an attempt was made to modify the Shtrikman-Wohlfarth model by taking into account the distribution of the superexchange interaction. The result obtained by the theoretical approach was applied to some oxide and fluoride glasses containing iron ions.

2. Theory

According to Shtrikman and Wohlfarth[9,10], the spin-freezing temperature T_f, which corresponds to the so-called blocking temperature in superparamagnetism, is expressed by the next equation in the weak coupling regime, i. e., the intercluster interaction is much weaker than the anisotropy field:

$$\tau=\tau_0\exp[(Kv+H_iMv)/kT_f], \tag{1}$$

where k is the Boltzmann constant, K and v are the uniaxial anisotropy and the volume of the superparamagnetic cluster, τ is the relaxation time for rotating the cluster, M is the saturation magnetization, and H_i is the intercluster interaction field. For the assembly of the clusters, H_i can be replaced by a statistical mean value $\langle H_i\rangle$ which is given

by

$$\langle H_i \rangle = H_i \tanh \frac{H_i M v}{kT} \sim \frac{H_i^2 M v}{kT} \tag{2}$$

for weak interactions. From Eqs. (1) and (2), the next equation holds:

$$\tau = \tau_0 \exp\left[\left(Kv + \frac{H_i^2 M^2 v^2}{kT_f}\right) / kT_f\right] \tag{3}$$

Eq. (3) is one result of the Shtrikman-Wohlfarth model. Here we can assume that

$$H_i = mJ \tag{4}$$

where J is the magnitude of the superexchange interaction and m is a positive constant. From Eqs. (3) and (4),

$$M^2 v^2 m^2 J^2 = k^2 T_f^2 \ln(\tau / \tau_0) - kT_f Kv > 0 \tag{5}$$

is derived. It is readily found from Eq. (5) that

$$\frac{\partial T_f}{\partial J} = \frac{M^2 v^2 m^2}{2k^2 T_f \ln(\tau / \tau_0) - kKv} > 0 \tag{6}$$

Therefore, the spin-freezing temperature increases monotonically with the increase of the magnitude of the superexchange interaction.

On the other hand, in the strong coupling regime, i. e., the intercluster interaction field is much stronger than the anisotropy field, the Ornstein-Zernike theory is applied so as to describe the correlation of spins. Hence, the effective volume of the cluster within which the spins correlate is expressed as follows[9),10)]:

$$v_{eff} = 4\pi \int r^2 \rho(r/\xi)\,(r/\xi_0)^{-1} dr, \tag{7}$$

where ξ is the correlation length given by

$$\xi = \xi_0 [(T - T_0) / T_0]^{-1/2} \tag{8}$$

with T_0 being an ordering temperature of the ensemble spins over the clusters. Eqs. (7) and (8) lead to the next equation:

$$v_{eff} = \varepsilon \xi_0^3 [(T - T_0) / T_0]^{-1}, \tag{9}$$

where

$$\varepsilon = 4\pi \int_0^\infty X e^{-X} dX = 4\pi \tag{10}$$

$\varepsilon \xi_0^3$ is roughly equal to v/p, where p is the volume packing fraction.

The anisotropy constant as well as the volume of the cluster has a temperature dependence. In the Shtrikman-Wohlfarth model, the anisotropy field is assumed to be randomly distributed and its statistical average value is deduced from the random walk model. Thus, the effective anisotropy constant is written as follows:

$$K_{eff} = pKN^{-1/2} = pK(v / pv_{eff})^{1/2}, \tag{11}$$

where N is the number of cluster in the correlated volume. From the above equations, the next equation is derived:

$$\tau=\tau_0\exp\{Kv[(T_f-T_0)/T_0]^{-1/2}/kT_f\} \tag{12}$$

This is the result deduced in the strong coupling regime. In this case, it can be assumed that

$$T_0=nJ, \tag{13}$$

where n is a positive constant. From Eqs. (12) and (13), the next relation results:

$$nJ=P^2T_f^3/(1+P^2T_f^2), \tag{14}$$

where $P=k\ln(\tau/\tau_0)/(Kv)$. Eq. (14) leads to the next relation:

$$\frac{\partial T_f}{\partial J}=\frac{n(1+P^2T_f^2)^2}{3+P^2T_f^2}>0. \tag{15}$$

Therefore, the spin-freezing temperature increases monotonically with the increase of the magnitude of the superexchange interaction also in this case.

In the present oxide and fluoride glass systems, a distribution of the superexchange interaction exists because of the distribution of Fe-O-Fe and Fe-F-Fe bond angles[11)-13)] Hence, the effect of the distribution of J should be introduced into Eqs. (3) and (12) for the construction of the model which can describe the practical system more appropriately. In the weak coupling regime, by using the distribution function $f(J)$, $\langle H_i\rangle$ is rewritten as the mean value in the first approximation:

$$\langle H_i\rangle=\int\frac{H_i^2Mv}{kT}f(J)dJ, \tag{16}$$

where $f(J)$ is the distribution function of the superexchange interaction. By using Eq. (16), the next equation is derived instead of Eq. (3):

$$\tau=\tau_0\exp\left[\left(Kv+\int\frac{m^2M^2v^2J^2}{kT_f}f(J)dJ\right)/kT_f\right]. \tag{17}$$

On the other hand, in the strong coupling regime, by replacing the spin correlation length with its average value given by

$$\xi=\xi_0\int[(T-T_0)/T_0]^{-1/2}f(J)dJ, \tag{18}$$

Eq. (12) is rewritten as follows:

$$\tau=\tau_0\exp\{Kv\int[(T_f-nJ)/nJ]^{-1/2}f(J)dJ/kT_f\}. \tag{19}$$

By using Eqs. (17) and (19), the relation between the spin-freezing temperature and the magnitude of the superexchange interaction can be derived in the case that a distribution of the superexchange interaction exists. Here, it is assumed that either the ferromagnetic or the antiferromagnetic interaction is dominant in the system. The situation of a coexistence of these two interactions is not considered.

For the weak coupling regime, we consider a function which has a symmetry axis of $J=J_0$ as the distribution function. From Eq. (17) along with the next relations

$$J-J_0=x,\ J_0/\Delta J=j,\ \text{and}\ T_f/\Delta J=t, \tag{20}$$

the next equation is derived:

$$A_1-A_2/t=\frac{2}{t^2}\int_{-\Delta J}^{\Delta J}\left(\frac{x^2}{\Delta J^2}+2\frac{x}{\Delta J}j+j^2\right)F(x)dx, \tag{21}$$

where $F(x)=f(J)$ for $x=J-J_0$ and A_1 and A_2 are positive constants given by

$$A_1=\frac{2k^2\ln(\tau/\tau_0)}{m^2M^2v^2},\ A_2=\frac{2kK}{m^2M^2v\Delta J}. \tag{22}$$

Since

$$f(J_0+y)=f(J_0-y) \tag{23}$$

for any y, we obtain

$$F(y)=F(-y). \tag{24}$$

Namely, $F(x)$ is an even function. Therefore, Eq. (21) results in the next equation:

$$A_1t^2-A_2t=4j^2\int_0^{\Delta J}F(x)dx+\frac{4}{\Delta J^2}\int_0^{\Delta J}x^2F(x)dx. \tag{25}$$

Since $F(x)>0$ for $0<x<\Delta J$, the two integrals on the right hand of Eq. (25) give positive values. Hence,

$$\frac{\partial t}{\partial j}=\frac{8j\int_0^{\Delta J}F(x)dx}{2A_1t-A_2}>0, \tag{26}$$

which leads to

$$\frac{\partial T_f}{\partial J_0}>0. \tag{27}$$

For the strong coupling regime, it seems instructive to examine the different distribution functions for the analysis of Eq. (19), because the quantitative analysis of the general function $f(J)$ is difficult. Here, three types of distribution functions are chosen. The first one is the delta function-like distribution expressed by the next equation:

$$f(J)=\begin{cases}1/2\Delta J & (J_0-\Delta J\leqq J\leqq J_0+\Delta J)\\ 0 & (\text{otherwise})\end{cases}, \tag{28}$$

where J_0 and ΔJ are the average value and distribution width of the magnitude of the superexchange interaction. The assumption that either the ferromagnetic or antiferromagnetic interaction exists results in $J_0>0$, $\Delta J>0$ and $J_0-\Delta J>0$. The schematic illustration for this distribution function is given in Fig. 1. By substituting Eq. (28) into Eq. (19) and setting that

$$J/\Delta J=x,\ J_0/\Delta J=j,\ \text{and}\ T_f/n\Delta J=t, \tag{29}$$

the next equation is derived:

$$B_1=\frac{1}{t}\int_{j-1}^{j+1}[(t-x)/x]^{-1/2}dx, \tag{30}$$

terer B_1 is a positive constant given by

$$B_1=\frac{2kn\Delta J\ln(\tau/\tau_0)}{Kv} \tag{31}$$

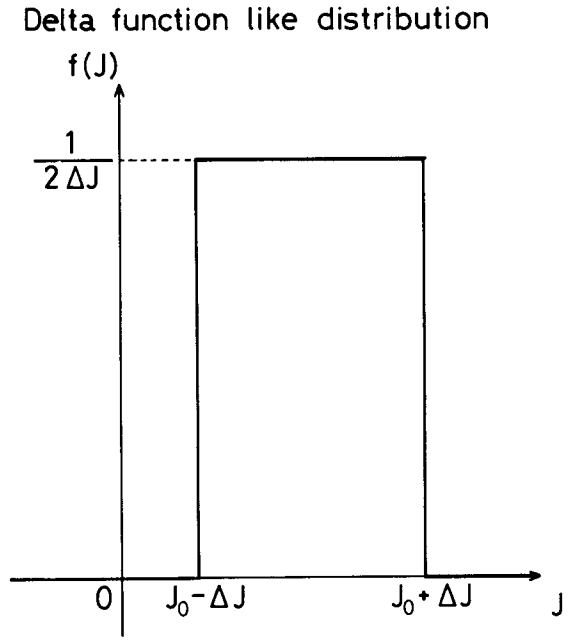

$$f(J) = \begin{cases} \dfrac{1}{2\Delta J} & (J_0 - \Delta J \leq J \leq J_0 + \Delta J) \\ 0 & (\text{otherwise}) \end{cases}$$

Fig. 1 Schematic illustration of the delta function-like distribution.

After the calculation of the integral in Eq. (30), the next relation is derived:

$$\frac{\partial j}{\partial t} = \frac{1}{1 - \dfrac{\sqrt{(j+1)(t-j-1)} - \sqrt{(j-1)(t-j+1)}}{t[\sqrt{(j+1)/(t-j-1)} - \sqrt{(j-1)/(t-j+1)}]}} \tag{32}$$

It is algebraically proved that

$$\frac{\partial j}{\partial t} > 0. \tag{33}$$

Hence, Eq. (27) holds also in this case.

Next, a parabolic distribution is considered. The distribution function is given as follows:

$$f(J) = \begin{cases} -(3/4\Delta J^3)[(J-J_0)^2 - \Delta J^2] & (J_0 - \Delta J \leqq J \leqq J_0 + \Delta J) \\ 0 & (\text{otherwise}) \end{cases} \tag{34}$$

The distribution is schematically drawn in Fig. 2. Firstly, the weak coupling regime is taken into account. In this case, the numerical calculation was performed. By substitut-

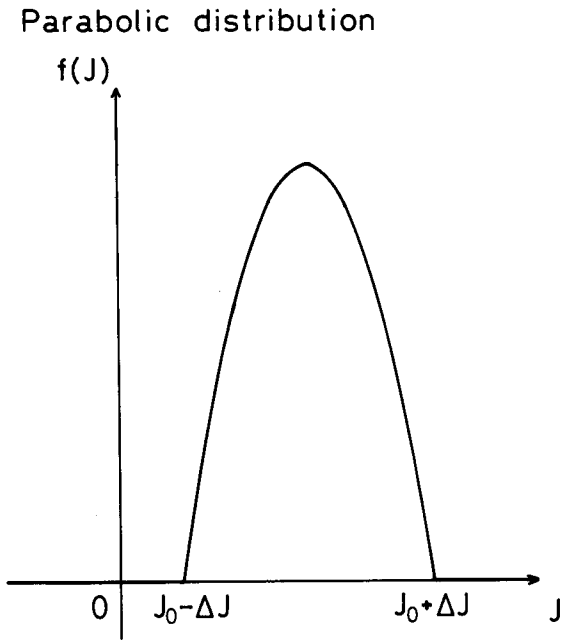

$$f(J)=\begin{cases}-\dfrac{3}{4\Delta J^3}\left[(J-J_0)^2-\Delta J^2\right] & (J_0-\Delta J\leqslant J\leqslant J_0+\Delta J)\\ 0 & (\text{otherwise})\end{cases}$$

Fig. 2 Schematic illustration of the parabolic distribution.

ing Eq. (34) into Eq. (19) and setting that

$$(J-J_0)/\Delta J=x,\ J_0/\Delta J=j,\ \text{and}\ T_f/n\Delta J=t, \tag{35}$$

the next equation is derived:

$$B_1=\frac{3}{2t}\int_{-1}^{1}[(t-j-x)/(j+x)]^{-1/2}(1-x^2)\,dx, \tag{36}$$

were B_1 is given in Eq. (31). The relation between t and j for the arbitrary value of B_1 numerically calculated is drawn in Fig. 3. It is seen that t increases monotonically with j, indicating that Eq. (27) holds.

Finally, the Gaussian distribution

$$f(J)=(1/\sqrt{2\pi}\,\Delta J)\exp\{-[(J-J_0)/\sqrt{2}\,\Delta J]^2\} \tag{37}$$

is adopted. In this case, the numerical calculation was carried out in the same way as the case of the parabolic distribution, where the range of the magnitude of the superexchange interaction was restricted to $J_0-3\Delta J\leqq J\leqq J_0+3\Delta J$. This is because the integral

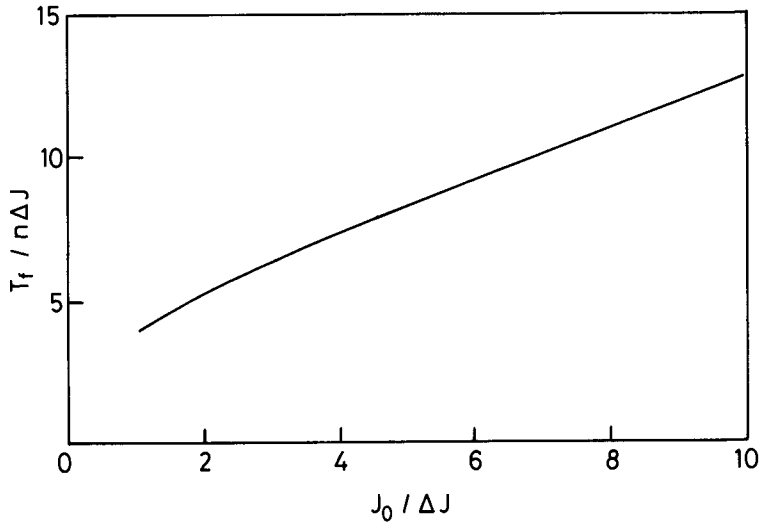

Fig. 3 Relation between $J_0/\Delta J$ and $T_f/n\Delta J$ calculated for parabolic distribution of J.

of the Gaussian function for this interval can be approximated to be equal to unity. Besides, $J_0-3\Delta J>0$ was assumed since either the ferromagnetic or the antiferromagnetic interaction is taken into account in the present calculations. By substituting Eq. (37) into Eq. (19) and setting

$$(J-J_0)/\Delta J=x,\ J_0/\Delta J=j,\ \text{and}\ T_f/n\Delta J=t, \tag{38}$$

the next equation is derived:

$$B_1=\frac{2}{t}\int_{-3}^{3}[(t-j-x)/(j+x)]^{-1/2}\frac{1}{\sqrt{2\pi}}\exp(-x^2/2)dx. \tag{39}$$

The relation between $j=J_0/\Delta J$ and $t=T_f/n\Delta J$ is drawn in Fig. 4. It is seen that t increases monotonically with increasing j. Therefore, Eq. (27) also holds for this case. For all types of distributions of J examined here, it is indicated that T_f increases as J_0 increases in both the weak and strong coupling regimes. Namely, the stronger the mean value of the superexchange interaction becomes, the higher the freezing temperature is. This leads to the expectation that T_f increases by increasing the covalency of $Fe^{3+}-O$ and $Fe^{3+}-F$ bonds for the glasses containing the same amount of Fe^{3+} ions since the superexchange interaction between Fe^{3+} ions is known to be proportional to the covalency of these bonds[14)-16)]. Hence, the difference of T_f due to the variation of the glass systems can be explained in terms of the covalency within the framework of the present model when the effects of the other factors such as the magnetic anisotropy field and the size of clusters are small.

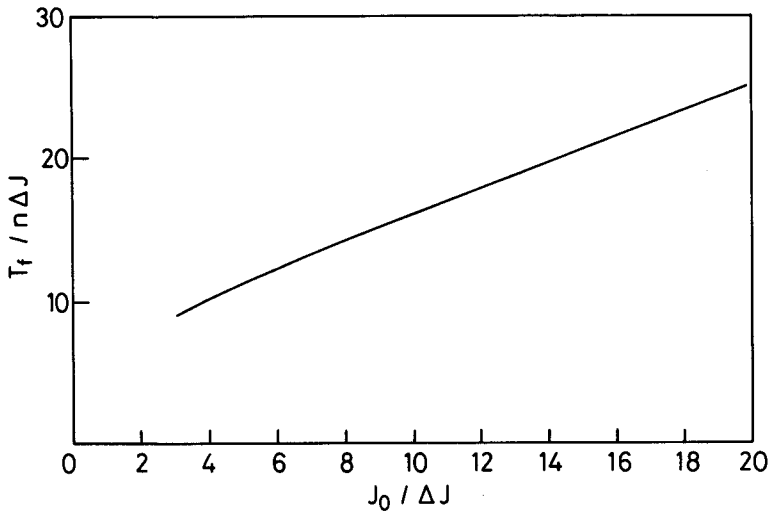

Fig. 4 Relation between $J_0/\Delta J$ and $T_f/n\Delta J$ calculated for Gaussian distribution of J.

3. Discussion

3. 1 Glass composition dependence of spin-freezing temperature

As mentioned above, the spin-freezing temperature increases by increasing the covalency when the other conditions such as the magnetic anisotropy energy and the concentration of the magnetic ions are identical. The isomer shift appearing in the

Table 1 The spin-freezing temperature (T_f) and the isomer shift (IS) for iron-based oxide and fluoride glasses

Glass composition	T_f(K)	Ref.*	IS(mm/s)	Ref.**
$39Fe_2O_3 \cdot 48BaO \cdot 13B_2O_3$	70[a]	19)	0.24	20)
$30Fe_2O_3 \cdot 45BaO \cdot 25B_2O_3$	14[b], 38[c]	22)	0.25	21)
$11.8Fe_2O_3 \cdot 29.4PbO \cdot 58.8B_2O_3$	4.0[d]	23)	0.36	this work
$11.9Fe_2O_3 \cdot 45.2Li_2O \cdot 42.9B_2O_3$	3.3[e], 7[a]	24)	0.28	this work
$44Fe_2O_3 \cdot 56P_2O_5$	7[g]	25)	0.41	this work
$Y_3Fe_5O_{12}$	40[g]	26)	0.31	26)
Fe_2O_3	80	27)	0.32	27)
$PbMnFeF_7$	11.77[f]	28), 29)	0.45	30)
Pb_2MnFeF_9	5.26[f]	28), 29)	0.43	30)

*References for the spin-freezing temperature, **References for the isomer shift value, a: Mössbauer effect, b : thermoremnant effect, c-f : ac susceptibility (c : 70Hz, d : 83Hz, e : 17.3Hz, f : 75Hz), g : de susceptibility

Mössbauer spectrum is closely related to the covalency of $Fe^{3+}-O$ and $Fe^{3+}-F$ bonds[17),18)], being able to be used as a good parameter of the covalency. In Table 1, the values of the isomer shift for some iron-based oxide and fluoride glasses studied so far[19)-30)] are summarized as well as the spin-freezing temperature. The isomer shifts for $44Fe_2O_3 \cdot 56P_2O_5$, $11.8Fe_2O_3 \cdot 29.4PbO \cdot 58.8B_2O_3$ and $11.9Fe_2O_3 \cdot 45.2Li_2O \cdot 42.9B_2O_3$ glasses are the new data measured in the present work. These oxide glasses were prepared by using Fe_2O_3, PbO, Li_2CO_3, B_2O_3 and $(NH_4)_2HPO_4$ as the raw materials. They were mixed and melted at 1000 to 1200°C in air. The melt was quenched with a

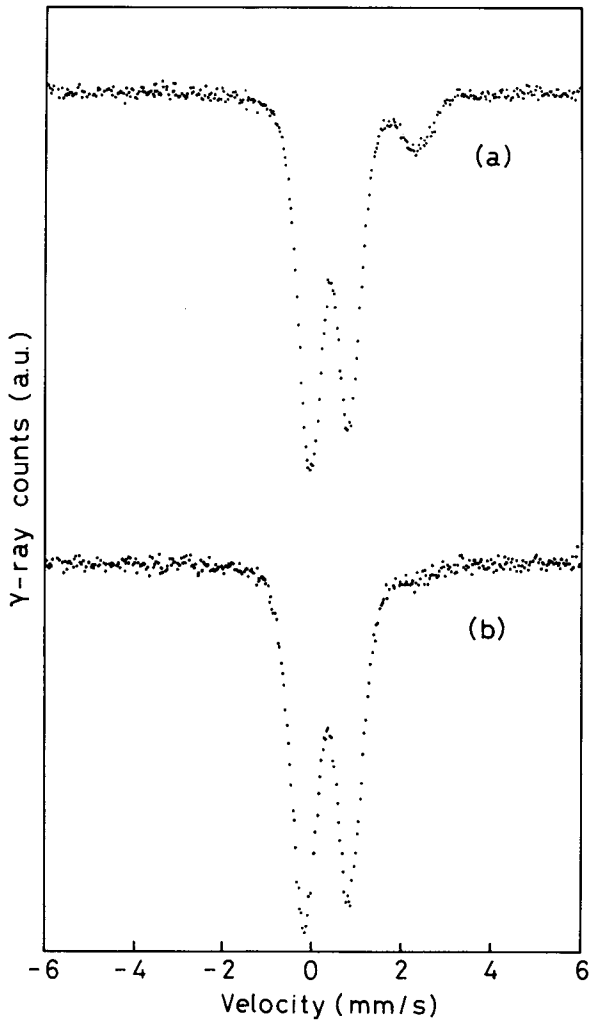

Fig. 5 Mössbauer spectra for (a) $44Fe_2O_3 \cdot 56P_2O_5$ and (b) $11.9Fe_2O_3 \cdot 45.2Li_2O \cdot 42.9B_2O_3$

twin-roller for the lithium borate glass and with an iron plate for the other glasses. The Mössbauer measurements were carried out at room temperature by using a 370 MBq ^{57}Co in Rh as the γ-ray source. The calculation of the isomer shift was done by using the spectrum of α-Fe foil at room temperature. Representative Mössbauer spectra for $44Fe_2O_3 \cdot 56P_2O_5$ and $11.8Fe_2O_3 \cdot 29.4PbO \cdot 58.8B_2O_3$ glasses are shown in Fig. 5. It is seen that the major part of the iron ions are in Fe(III) state in these oxide glasses.

The relation between the spin-freezing temperature and the isomer shift value for those materials in Table 1 is shown in Fig. 6. In order to take into consideration the difference in the concentration of iron ions among these amorphous oxides, the term $T_f/(c-c')$, where c stands for the concentration of iron ion expressed as the atomic ratio of the cation and c' corresponds to the concentration where T_f becomes zero, is plotted as

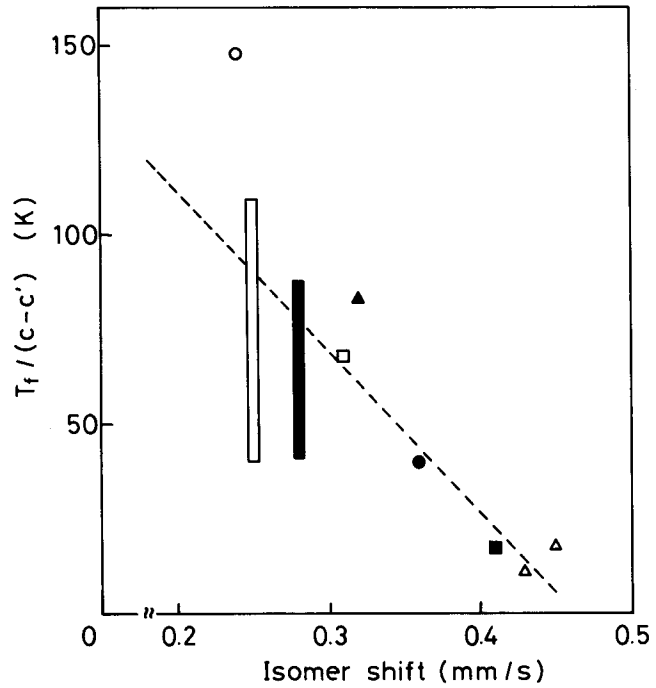

Fig. 6 Relation between the spin-freezing temperature and the isomer shift for Fe^{3+}—containing insulating glasses. Since the spin-freezing temperature is dependent on the method of measurements, the temperature range where the spin-freezing is observable is indicated for a few of the glasses. The broken line is to guide the eyes. (○ and open bar : Fe_2O_3—BaO—B_2O_3, closed bar : Fe_2O_3—Li_2O—B_2O_3, ● : Fe_2O_3—PbO—B_2O_3, □ : Y_2O_3—Fe_2O_3, ■ : Fe_2O_3—P_2O_5, ▲ : Fe_2O_3, △ : PbF_2—MnF_2—FeF_3)

ordinate in this figure. The parameter c' presents also the concentration where the clusters of iron ions start to form in the glass. The value of c' has been estimated for several oxide glass systems. For example, Mendiratta et al.[23] found c' to be 0.036 for the Fe_2O_3—NiO—PbO—B_2O_3 system by applying ac susceptibility measurements. Moon et al.[31] examined the formation of the cluster of Fe^{3+} ions in Fe_2O_3—BaO—B_2O_3 glasses by means of magnetization and ESR measurements and estimated $c'=0.033$. For the Fe_2O_3—Li_2O—B_2O_3 system, $c'=0.061$ was revealed by Mössbauer measurements at 4.2K[24] In the present study, the value of c' is assumed to be 0.04, which is compatible with above-mentioned values. The parameter $T_f/(c-c')$ is considered appropriate as the first approximation, because the linear relation between T_f and $c-c'$ was experimentally observed for the cluster spin glasses[32),33)]. The trend that $T_f/(c-c')$ increases with a decrease of the isomer shift seen from Fig. 6 indicates that the spin-freezing temperature increases with an increase of the covalency or the superexchange interaction between iron ions. Thus, the present model seems to be appropriate for describing the effect of glass composition on the spin-freezing temperature for these iron-based oxide and fluoride glasses.

3. 2 Measuring frequency dependence of spin-freezing temperature

It is known that Vogel-Fulcher empirical law[34),35)] well describes the relation between the spin-freezing temperature and the measuring frequency for iron-based oxide and fluoride glasses[23),24),36)-38)] as well as metallic spin glasses[39)]. Namely, the measuring frequency ν is related to the spin-freezing temperature as follows:

$$\nu=\nu_0\exp\left[-\frac{E}{k(T_f-T_0)}\right], \tag{40}$$

where E is the activation energy for the rotation of the magnetic moment within the cluster. When this equation is applied for the data of $11.9Fe_2O_3\cdot 45.2Li_2O\cdot 42.9B_2O_3$ glasses, T_0 becomes 2.7 K[24].

In the present model, the relation between the spin-freezing temperature and the measuring frequency is represented as the next form for the weak coupling regime:

$$\nu=\nu_0\exp\left[-\left(E_K+\frac{E_i^2}{kT_f}\right)/kT_f\right], \tag{41}$$

where

$$E_K=Kv=kT_K \tag{42}$$

and

$$E_i^2=\int (mMvJ)^2 f(J)\,dJ. \tag{43}$$

When T_0 is defined as

$$kT_0=E_i^2/E_K, \tag{44}$$

Eq. (41) is transformed into the next equation for $T_0/T_K\gg 1$ which is the condition for

the weak coupling regime:

$$\nu=\nu_0\exp[-Kv/k(T_f-T_0)]. \tag{45}$$

Eq. (45) is identical to Eq. (40), that is, the Vogel-Fulcher law.

On the other hand, the measuring frequency dependence of the spin-freezing temperature depends on the distribution function of the superexchange interaction for the strong coupling regime. Here, we pay attention to only the delta function-like distribution. In this case, the measuring frequency dependence of the spin-freezing temperature is represented by Eq. (30). By using this equation with appropriate values for B_1 and $J_0=3.0\,K$, the experimental data of $11.9Fe_2O_3 \cdot 45.2Li_2O \cdot 42.9B_2O_3$ glasses can be well analyzed. The result of the analysis is illustrated in Fig. 7. The value of J_0 obtained is almost identical to T_0 given when Eq. (40) is applied[24]. As clearly seen from this figure, the agreement of the experimental data and the curve calculated from Eq. (30) is rather good.

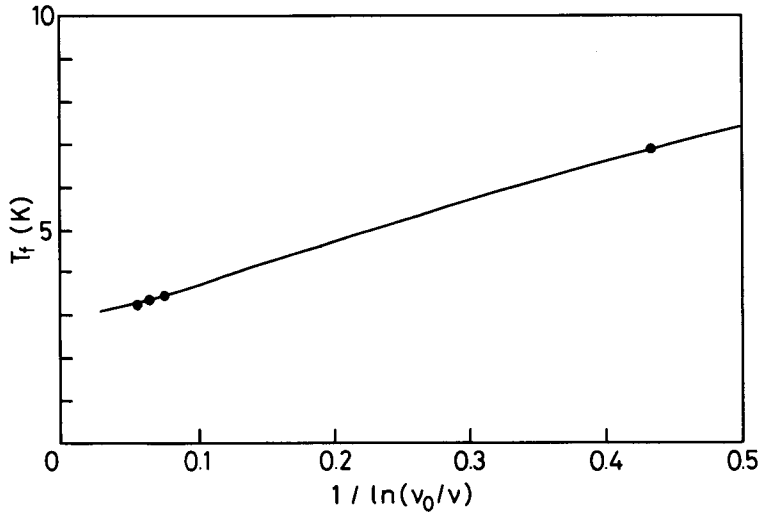

Fig. 7 The measuring frequency dependence of the spin-freezing temperature for $11.9Fe_2O_3 \cdot 45.2Li_2O \cdot 42.9B_2O_3$ glasses. The solid curve is drawn by using Bq. (30) (see text).

Figure 8 shows the result of a similar analysis on $51.8FeO \cdot 5.8Al_2O_3 \cdot 42.4SiO_2$ glasses[38]. Here, $J_0=7.6$ K was used when the data were analyzed. The good agreement between the experimental data and the calculated curve is observable. Thus, it is concluded that the present model is also effective for the explanation of the measuring frequency dependence of the spin-freezing temperature for the strong coupling regime as well as for the weak coupling regime.

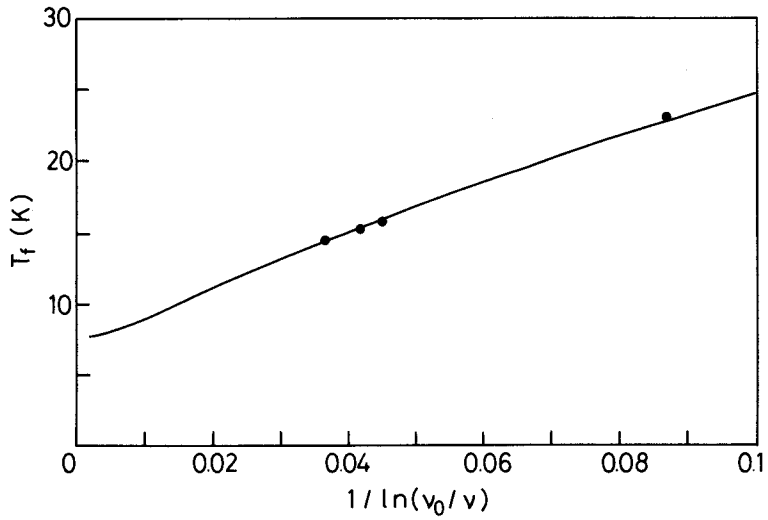

Fig. 8 The measuring frequency dependence of the spin-freezing temperature for $51.8FeO \cdot 5.8Al_2O_3 \cdot 42.4SiO_2$ glasses . The solid curve is drawn by using Eq. (30) (see text).

4. Conclusion

In the present study, by analyzing the Shtrikman-Wohlfarth model, we derived the expectation that the spin-freezing temperature increases with an increase of the covalency of Fe—O and Fe—F bonds in oxide and fluoride glasses when the content of iron ions is identical. The relationship between the spin-freezing temperature observed experimentally and the isomer shift obtained from the Mössbauer effect measurements described seems to support this expectation qualitatively. It was also found that the present model is effective for describing the measuring frequency dependence of the spin-freezing temperature. The Vogel-Fulcher law modified within the framework of the present model was well applied to explain the experimental data of the measuring frequency dependence of the spin-freezing temperature for some oxide glasses. The value of the intercluster interaction parameter T_0 obtained by analyzing the experimental data on the basis of the present model is physically meaningful.

5. Acknowledgement

The present authors would like to thank Dr. Y. Isozumi of the Radioisotope Research Center, Kyoto University for the Mössbauer measurements.

References

1) R. A. Verhelst, R. W. Kline, A. M. de Graaf and H. O. Hooper, Phys. Rev., **B11**, 4427 (1975)
2) H. R. Rechenberg, L. H. Bieman, F. S. Huang and A. M. de Graaf, J. Appl, Phys., **49**, 1638 (1978)
3) J. P. Jamet, J. C. Dumais, J. Seiden and K. Knorr, J. Magn. Magn. Mat., **15-18**, 197 (1980)
4) E. P. Wohlfarth, J. Phys., **F10**, L241 (1980)
5) S. K. Burke, R. Cywinski, J. R. Davis and B. D. Rainford, J. Phys., **F13**, 451 (1983)
6) L. Néel, Rev. Mod. Phys., **25**, 293 (1953)
7) T. Goto and T. Kanomata, J. Appl. Phys., **57**, 3450 (1985)
8) J. P. Sanchez, J. M. Friedt, R. Horne and A. J. van Duyneveldt, J. Phys., **C17**, 127 (1984)
9) S. Shtrikman and E. P. Wohlfarth, Phys. Lett., **85A**, 467 (1981)
10) S. Shtrikman and E. P. Wohlfarth, J. Magn. Magn. Mat., **31-34**, 1421 (1983)
11) G. Ferey, F. Varret and J. M. D. Coey, J. Phys., **C12**, L531 (1979)
12) M. E. Lines, Phys. Rev., **B20**, 3729 (1979)
13) M. Eibschütz, M. E. Lines, L. G. van Ultert, H. J. Guggenheim and G. J. Zydzik, Phys. Rev., **B29**, 3843 (1984)
14) P. W. Anderson, Phys. Rev., **79**, 350 (1950)
15) J. Kanamori, Magnetism (Baifukan Ltd., Tokyo, 1969), p. 56 (in Japanese)
16) J. Kanamori, J. Phys. Chem. Solids, **10**, 87 (1959)
17) L. R. Walker, G. K. Wertheim and V. Jaccarino, Phys. Rev. Lett., **6**, 98 (1961)
18) J. Danon, Lectures on the Mössbauer Effect (Gordon & Breach, New York, 1968), p. 92
19) Y. Syono, A. Ito and O. Horie, J. Phys. Soc. Jpn., **46**, 793 (1979)
20) O. Horie, Y. Syono, Y. Nakagawa, A. Ito, K. Okamura and S. Yajima, Solid State Commun., **25**, 423 (1978)
21) A. Bonnenfant, J. M. Friedt, M. Maurer and J. P. Sanchez, J. de Phys., **43**, 1475 (1982)
22) H. Laville and J. C. Bernier, J. Mat. Sci., **15**, 73 (1980)
23) S. K. Mendiratta, R. Horne and A. J. van Duyneveldt, Solid State Commun., **52**, 371 (1984)
24) J. P. Sanchez and J. M. Friedt, J. de Phys., **43**, 1707 (1982)
25) T. Egami, O. A. Sacli, A. W. Simpson, A. L. Terry and F. A. Wedgwood, J. Phys., **C5**, L261 (1972)
26) E. M. Gyorgy, K. Nassau, M. Eibschütz, J. V. Waszczak, C. A. Wang and J. C. Shelton, J. Appl. Phy., **50**, 2883 (1979)
27) A. M. van Diepen and Th. J. A. Popma, Solid State Commun., **27**, 121 (1979)
28) J. P. Renard, J. P. Miranday and F. Varret, Solid State Commun., **35**, 41 (1980)
29) J. P. Renard, C. Dupas, E. Velu, C. Jacoboni, G. Fonteneau and J. Lucas, Physica, **108B**, 1291 (1981)
30) Y. Kawamoto, J. Fujiwara, K. Hirao and N. Soga, J. Non-Cryst. Solids, **95-96**, 921 (1987)
31) D. W. Moon, J. M. Aitken, R. K. MacCrone and G. S. Cieloszyk, Phys. Chem. Glasses, **16**, 91 (1975)
32) V. Cannella and J. A. Mydosh, Phys. Rev., **B26**, 4220 (1972)
33) M. K. Hou, M. B. Salamon and M. J. Pechan, J. Appl. Phys., **57**,3482 (1985)
34) H. Vogel, Z. Phys., **22**, 645 (1921)
35) G. S. Fulcher, J. Am. Ceram. Soc., **8**, 339 (1925)
36) P. Beauvillain, C. Dupas, J. P. Renard and P. Veillet, J. Magn. Magn. Mat., **31-34**, 1377 (1983)

37) A. T. Meert and L. E. Wenger, J. Magn. Magn. Mat., **23**, 165 (1981)
38) J. P. Sanchez, J. M. Friedt, R. Horne and A. J. van Duyneveldt, J. Phys., C**17**, 127 (1984)
39) J. L. Tholence, Solid State Commun., **35**, 113 (1980)